# Supersymmetry at the LHC and Beyond -Ultimate Targets—

Mihoko M. Nojiri

YITP, Kyoto University
Sakyo, Kyoto, 606-8502 Japan
E-mail: nojiri@yukawa.kyoto-u.ac.jp

#### ABSTRACT

At the LHC, superpartners with the masses lighter than a few TeV may be found, and the masses of the supersymmetric (SUSY) particles and their interactions will be studied. The information will be the base to consider the SUSY breaking mechanism and cosmology related to the SUSY dark matter. We review the recent studies that aims for the "precise SUSY study" at the LHC.

## 1. Introduction

The LHC experiment, scheduled to start from 2007, is the best place to study the supersymmetry in coming 10 years. The LHC is a pp collider at  $\sqrt{s} = 14$  TeV. It is able to find  $\tilde{q}$  and  $\tilde{g}$  in the minimal supersymmetric standard model(MSSM) up to 2–3 TeV. Not only for that, it is also the place to do the precise measurement of the nature of the SUSY particles. If the sparticle masses are as light as 1 TeV, the production cross section is as large as 3 pb, therefore O(10000) events /year will be produced for the detailed study. It is our responsibility to extract physics information, as much as possible, from the LHC experiment for the future developments of the experimental and theoretical particles physics.

Different SUSY breaking models leave special imprints to the mass spectrums, therefore measurement of the masses of the SUSY particles is a important target for the collider physics. After finding superpartners, we can select pure samples of the SUSY events free from standard model (SM) backgrounds. By looking into the distributions of the sparticle decay products, we can determine the mass of the sparticles, which may provide us the understanding of the SUSY breaking mechanism, namely, physics at the very high scale.

The measurements also have impacts to the other physics. The mass spectrum determination constrains the SUSY contributions to the flavor violating processes, such as b rare decays,  $\mu \to e\gamma$ , and muon anomalous magnetic moment. The thermal relic density of the SUSY dark matter also can be calculated if the MSSM parameters are known.

One may even study some of the SUSY relations. In the MSSM, the chiral structure of the coupling of the superpartners are restricted. For example the bino and wino couplings are the (s)fermion chirality conserved form  $f_{L(R)}\tilde{f}_{L(R)}\tilde{B}$  or  $f_L\tilde{f}_L\tilde{W}$ . The sparticle left-right mixing are induced by the F term as  $(m^2)^{LR}_{\tilde{l}} \propto m_l \mu \tan \beta$ . We will discuss how to prove such relations at the LHC for explicit examples.

Before going into the detail, let us first summarize basic features of the collider signatures of the SUSY particles at the LHC. In the models where SUSY is broken at high energy scale, the squark and gluino masses are much higher than that of the weak interacting SUSY particles. Therefore, at least one jet originated from a squark or a gluino

cascade decay has large  $p_T$ . The decay products include weakly interacting SUSY particles, which further decay into the leptons or jets. Especially, at the end of each sparticle cascade decay, the lightest SUSY particle (LSP) appears, which may be stable due to the R parity conservation. The LSP cannot be detected in the detector, therefore SUSY events have large missing momentum. By applying the cuts on the missing  $P_T$  and the total transverse energy  $M_{\text{eff}}$ , the SM backgrounds can be reduced to the negligible level.

One of the relatively clean channels is the 2 body cascades or 3 body decays of the heavier neutralinos  $\tilde{\chi}_i^0$  which have been obtained lots of attentions in the past physics performance studies[1],

$$\tilde{\chi}_i^0 \to (\tilde{l}l) \to ll \tilde{\chi}_1^0.$$
 (1)

The cascade decay produce opposite sign same flavor leptons(OSSF). The accidental leptons can be estimated from the  $e\mu$  distribution (opposite sign opposite flavor leptons—OSOF), leaving very clean samples containing  $\tilde{\chi}_i^0$ .

Another important SUSY channels are those containing b quarks. In many SUSY breaking models,  $\tilde{b}$  and  $\tilde{t}$  could be much lighter than other squarks because of the negative running of the squark mass by the Yukawa coupling, in addition to the left-right mixing. The decays  $\tilde{g} \to \tilde{b}, \tilde{t}$  are to open in the wide parameter space. The LHC detectors have a good tagging efficiency for b jets  $\epsilon_b \sim 0.5$ , and the cascade decays,

$$\tilde{g} \rightarrow b\tilde{b} \begin{cases} \tilde{b} \rightarrow \tilde{\chi}_{i}^{0}b \\ \tilde{b} \rightarrow \tilde{\chi}_{i}^{+}t \end{cases}$$

$$\tilde{g} \rightarrow t\tilde{t} \begin{cases} \tilde{t} \rightarrow \tilde{\chi}_{i}^{0}t \\ \tilde{t} \rightarrow \tilde{\chi}_{i}^{+}b \end{cases} \tag{2}$$

maybe studied at the LHC by tagging two b jets. In the next section, we will discuss these processes as well.

#### 2. Sparticle Mass Measurements at the LHC

If the LSP is stable, the SUSY events have large missing transverse momentum. This is important signature to discriminate it from the SM backgrounds. On this other hand, one has to determine the parent SUSY particle masses from the momentum of the visible particles only. This is easy for the case of  $e^+e^-$  collider experiments. The energy of collisions are known, and the decay kinematics can be solved by the constraint. But it is not simple task at the LHC, where a proton is a composite particle and collision energies of the partons are not fixed.

The techniques to do the jobs at the LHC have been developed in the past 10 years. We quickly review the previous works and also explain new ideas.

## 2.1. The case with the long lived NLSP

In the models with the gravitino LSP, the NLSP is long lived and could be either charged or neutral. The NLSP candidates are sleptons (especially the lighter stau  $\tilde{\tau}_1$ ), the

lightest neutralino  $\tilde{\chi}^0_1$ , or sneutrinos  $\tilde{\nu}$ . The NLSP could decay into its SM partner and a gravitino

$$\tilde{l} \rightarrow l\tilde{\psi}_{3/2}, 
\tilde{\chi}_1^0 \rightarrow \gamma \tilde{\psi}_{3/2}.$$
(3)

One can extract the mass of SUSY particles by measuring the endpoints of the invariant mass distributions of the selected particles involving the photon or lepton. (The endpoint method is discussed in the next section). For example, from the endpoint of the  $m_{\gamma l}$ ,  $m_{\gamma ll}$  and  $m_{ll}$  .. of the cascade decay  $\tilde{\chi}_2^0 \to \tilde{l}l \to \tilde{\chi}_1^0 ll \to \tilde{\psi}_{3/2} ll \gamma$ , one can calculate  $\tilde{\chi}_{1(2)}^0$  and  $\tilde{l}$  mass model independently with high precision of O(1) GeV. The structure of the messenger sector will be determined very precisely from the mass measurements.

The life time of the NLSP depends on the scale of the hidden sector SUSY breaking F which is also related to the gravitino mass  $m_{3/2} = F/(\sqrt{3}M_{\rm pl})$ . We may learn the structure of the hidden sector from the measurement of the life time. For example, the life time is given for the decay  $\tilde{l} \to l\tilde{\psi}_{3/2}$  as [2]

$$\tau_{\text{NLSP}} = \left(\frac{100 \text{GeV}}{m_{\text{NLSP}}}\right)^5 \left(\frac{\sqrt{F}}{100 \text{TeV}}\right)^4 3 \times 10^{-13} \text{sec.}$$
(4)

The gravitino could be a dark matter. It can be produced either thermally or from the NLSP decays. However if the life time of the NLSP is longer than 1 sec, the decay products may affect the BBN and effect depends on the life time strongly. The cosmology related to the gravitino is discussed in this workshop in detail[4,5].

The signature of the charged NLSP(CNLSP) would be very spectacular. It is detected as a highly ionizing particles as it is non-relativistic. The time of the flight(TOF) information at the muon systems and momentum measurement at the inner detector allows precise measurement of the NLSP mass[3]. All neutralino masses may be determined within the error of O(1) GeV by combining the NLSP momentum with that of the other visible particles.

The supergravity interaction may also be studied in detail for this case. The charged NLSP may travel through the detector with finite vertex until it decays finally. The life time can be calculated from the distribution of the flight distance and the decay time of the NLSP. It should be possible to do such measurements as far as they decays inside the detector, although there are no systematic experimental study on the expected precision of the lifetime at the LHC. Even if  $c\tau_{\rm NLSP}$  is longer than the detector scale, the stable charged particle may be stopped at the massive stopper placed nearby the main detector[4]. Recent study shows that one can determine the life time as long as O(100) years at LHC, if a massive stopper with mass around 1 kton can be placed near the LHC detectors[6,7].

For the neutral long lived NLSP, the NLSP momentum cannot be measured directly. If the life time is short enough, it decays into a photon and a gravitino in the detector, and the photon will be detected at the ECAL. The reconstruction of the NLSP momentum, a decay position and a decay time of the NLSP is possible event by event by using the

time information and photon momentum measurement at ECAL[8]. This is because nonrelativistic neutralinos fly in the detector then decay, therefore the arrival time depends on both the NLSP momentum and decay time. The resolution of the decay time and position depends on the time resolution of the ECAL. The ECAL time resolution is about O(0.1) nsec in a beam test, which corresponds to O(3cm) resolution on the NLSP vertex. Assuming the time resolution, the mass error obtained from the reconstructed NLSP momentum is estimated as low as O(1) GeV at a model point[8], for the process

$$\tilde{l} \to \tilde{\chi}_1^0 l \to \tilde{\psi}_{3/2} \gamma l.$$
 (5)

In the limit where the NLSP life time is too long to decay in the detector, the signature becomes very close to the case where the LSP is the lightest neutralino. This will be discussed in the next subsections.

### 2.2. The case with the lightest neutralino LSP at the LHC

When the lightest neutralino is stable, it is not possible to measure the momentum directly. The study of the mass spectrum is still possible by looking into the decay distribution of the visible particles from sparticle decays.

The past physics studies are mostly done with the endpoint method. Namely, one measures endpoints of the invariant mass distribution of the selected sample which are dominated by the events from a decay cascades. The positions of the endpoints depend on the sparticle masses. For example, the endpoint of the  $m(l^+l^-)$  distribution for the cascade decay given in Eq. (1) is

$$m_{ll}(3 \text{ body}) = m_{\tilde{\chi}_2^0} - m_{\tilde{\chi}_1^0},$$

$$m_{ll}(2 \text{ body}) = \sqrt{\frac{(m_{\tilde{\chi}_2^0}^2 - m_{\tilde{l}}^2)(m_{\tilde{l}}^2 - m_{\tilde{\chi}_1^0}^2)}{m_{\tilde{l}}^2}},$$
(6)

respectively. One can then select a jet from a squark decay  $\tilde{q} \to q \tilde{\chi}^0_2$  by taking one of the two highest  $p_T$  jets. The endpoint of the invariant mass of the jet and leptons provide the constraints among  $m_{\tilde{q}}$  and the lighter SUSY particle masses involved in the cascade decay.

For the point SPS1a which is defined in the mSUGRA scenario by the parameters  $\tan \beta = 10$ , m = 100 GeV, M = 250 GeV,  $A_0 = -100$  GeV, and  $\mu > 0$  [9], the error of sparticle masses at the LHC for the integrated luminosity  $\int \mathcal{L}dt = 300$  fb<sup>-1</sup> are estimated in [10], and the results are summarized in Table 1.

The cross section at SPS1a is large ( $\sigma \sim 58 \mathrm{pb}$ ) and  $O(10^6)$  sparticle will be produced at the high luminosity option of the LHC at this point. For weakly interacting particles, the errors are dominated by the uncertainty of the absolute mass scale, while the mass differences of the sparticles are more strongly constrained. This is general feature of the determination of the sparticle masses when the LSP momentum cannot be measured directly. The mass of the lightest neutralino may be measured more precisely at the international linear collider (ILC), then error of the sparticle masses would be reduced

sparticle	mass(GeV)	error (GeV)	with $m_{\tilde{\chi}_1^0}$ input	comment
$ ilde{g}$	595	8.0	6.4	bbll mode
$ ilde{q}_R$	520	11.8	10.9	use $M_{T2}$
$ ilde{q}_L$	540	8.7	4.9	jll  mode
$ ilde{b}_1$	492	7.5	5.7	bbll, need collect $b$ jet calibrations
$ ilde{b}_2$	525	7.9	6.3	to separate two $\tilde{b}$ 's
$ ilde{\chi}_4^0$	378	5.1	2.25	high $ll$ edge
$egin{array}{c}  ilde{\chi}_4^0 \  ilde{\chi}_2^0 \  ilde{l}_R \end{array}$	177	4.7	0.24	jll  mode
$ ilde{l}_R$	143	4.8	0.34	jll
$ ilde{\chi}_1^0$	96	4.8	N.A.	jll

Table 1: Mass of the sparticles at SPS1a, and expected sensitivity at the LHC, and that with the expected input from the ILC.

significantly as can be see the 4th column of the Table 1. Finally the errors for the squark and gluino masses are dominated by the 1% jet scaling error.

It is notable that the LHC can access to the mass of the the heaviest neutralino  $\tilde{\chi}_4^0$  through its decay into sleptons. For this model  $m_{\tilde{\chi}_4^0} = 378$  GeV, which cannot be accessible at  $\sqrt{s} = 500$  GeV  $e^+e^-$  colliders. The measured mass difference  $m_{\tilde{\chi}_4^0} - m_{\tilde{\chi}_1^0}$  directly constrains  $\mu$  parameter. The errors for the MSSM parameters would be significantly reduced when the measurements at the LHC and the ILC can be combined[11].

We also can see the implication to the cosmology. The mass of the slepton and the lightest neutralino can be determined within O(5)% level. This means one can calculate the neutralino pair annihilation rates into the first and second generation leptons at the time of decoupling with in the error of 10%. The pair annihilation rates into  $\tilde{\tau}$  is also important. The  $\tilde{\tau}$  mass also can be measured at the LHC, but more study is needed to obtain the error, as the channel involving  $\tau$  leptons suffers backgrounds from QCD jets.

#### 2.3. Mass relation method

Although the mass determination through the endpoint method is successful, there are problems which may limit the application. The problems may be summarize as follows;

- The LSP momentum cannot be reconstructed except for a few very special part of the decay phase space.
- Only the events near the endpoints of the decay distribution are used for the mass fit. The large statistics are required to see the endpoints while the events away from the endpoints also contain the independent information of the masses.
- The selected SUSY events may contain events from several cascade chains. For example, three or four channels involving  $\tilde{b}_i$  or  $\tilde{t}_i$  contribute simultaneously for *bbll* final state. The measured m(bbll), m(bll) and m(bl) endpoints are the weighted average of the endpoints of these channels. This introduces additional systematical uncertainty for the mass determinations.

$\tan \beta$	$m_{ ilde{g}}$	$m_{\tilde{b}_{1(2)}}$	$m_{ ilde{\chi}^0_2}$	$m_{ ilde{\ell}_R}$	$m_{ ilde{\chi}^0_1}$
10	595.2	491.9 (524.6)	176.8	143.0	96.0
15	595.2	485.3 (526.9)	177.9	143.0	96.5
20	595.2	478.7 (531.2)	178.5	143.1	96.7

Table 2: Masses of some sparticles at SPS1a and the variants studied in Section 3, in GeV.

The above problems may be removed by using the "mass relation method" [12,13] when a sparticle cascade decay chain is sufficiently long. In the mass relation method, one uses the on-shell condition of the sparticle masses to solve the kinematics of the sparticle decay product exactly, and reconstruct the masses of the SUSY particles as the peaks of certain distributions. To describe the method, let us take the process

$$\tilde{g} \to \tilde{b}b_2 \to \tilde{\chi}_2^0 b_1 b_2 \to \tilde{\ell}b_1 b_2 \ell_2 \to \tilde{\chi}_1^0 b_1 b_2 \ell_1 \ell_2,$$
 (7)

where  $b_1$ ,  $b_2$ ,  $l_1$  and  $l_2$  denote different b quarks and leptons respectively. Both of the sbottom states  $\tilde{b}_1$  and  $\tilde{b}_2$  yield the decay chain of Eq. (7).

Five sparticles are involved in the cascade decay Eq. (7), therefore one can write five mass shell conditions among the leptons and quarks in the final decay products.

$$m_{\tilde{\chi}_{1}^{0}}^{2} = p_{\tilde{\chi}_{1}^{0}}^{2},$$

$$m_{\tilde{\ell}}^{2} = (p_{\tilde{\chi}_{1}^{0}} + p_{\ell_{1}})^{2},$$

$$m_{\tilde{\chi}_{2}^{0}}^{2} = (p_{\tilde{\chi}_{1}^{0}} + p_{\ell_{1}} + p_{\ell_{2}})^{2},$$

$$m_{\tilde{b}}^{2} = (p_{\tilde{\chi}_{1}^{0}} + p_{\ell_{1}} + p_{\ell_{2}} + p_{b_{1}})^{2},$$

$$m_{\tilde{g}}^{2} = (p_{\tilde{\chi}_{1}^{0}} + p_{\ell_{1}} + p_{\ell_{2}} + p_{b_{1}} + p_{b_{2}})^{2}.$$
(8)

For a  $bb\ell\ell$  event, the equations contain the 4 unknown degrees of freedom of the  $\tilde{\chi}^0_1$  momentum. Each event therefore describes a 4-dimensional hyper-surface in a 5-dimensional mass parameter space, and the hyper-surface differs event by event. From the purely mathematical point of view 5 events would be enough to determine a discrete set of solutions for the masses of the involved sparticles.

From now on, we will develop the argument by assuming that the masses of  $\tilde{\chi}_2^0$ ,  $\tilde{\ell}$ , and  $\tilde{\chi}_1^0$  are known for simplicity. This is a reasonable assumption at the LHC, where it has been shown that a detailed study of the lepton-lepton system from the  $\tilde{\chi}_2^0$  decay can be used to precisely constrain these masses. In addition to that, if the international linear collider (ILC) would be build, the mass of lighter sparticles will be measured with less than 1% accuracy there. If we assume the mass of the lighter sparticles is known, each event corresponds to a different curve in the  $(m_{\tilde{g}}, m_{\tilde{b}})$  plane, which is expressed as following equation;

$$f(m_{\tilde{g}}, m_{\tilde{b}}, p_{b1}, p_{b2}, p_{l1}, p_{l2}) = Q_{11}m_{\tilde{g}}^4 + 2Q_{12}m_{\tilde{g}}^2m_{\tilde{b}}^2 + Q_{22}m_{\tilde{b}}^4 + 2Q_1m_{\tilde{g}}^2 + 2Q_2m_{\tilde{b}}^2 + Q = 0, \quad (9)$$

where Q's are the functions of the lighter sparticle masses and momenta of the b quarks and leptons. Two events are enough to solve the gluino and sbottom masses altogether up to the maximally four solutions. <sup>a</sup>

<sup>&</sup>lt;sup>a</sup>In addition, there are two possibility to assign the two leptons to  $l_1$  and  $l_2$ . In the plot of this paper, we fix the assignment by fixing the assignment so that the lepton with the higher  $p_T$  is  $l_1$ .

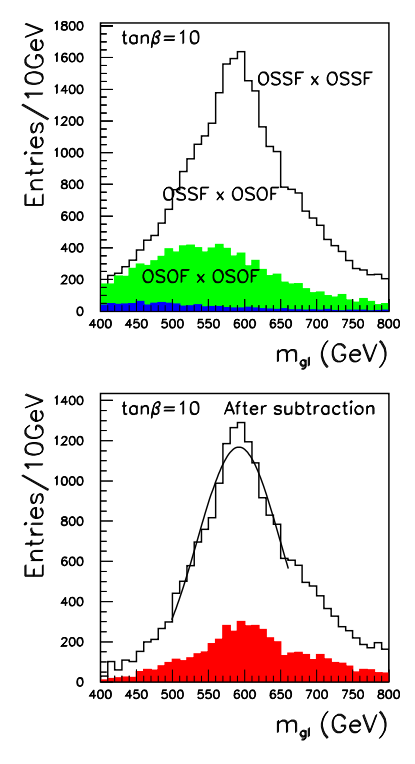


Figure 1: The gluino mass distributions for SPS1a with the event pair analysis. The open, green, and blue histograms in the top figures are for OSSF $\times$ OSSF, OSSF $\times$ OSOF, and OSOF $\times$ OSOF event pairs, respectively. The open histograms in the bottom figures shows the mass distributions after background subtraction. The contributions of  $b_2$  are shown by red histograms.

We call this technique "mass relation method", because here one uses the fact that the sparticle masses are common for all events which go though the same cascade decay chain. Note that the events need not to be close to the endpoint of the decay distribution, but they are still relevant to the mass determination. This means that one can use the mass relation method even if the number of signal events is small.

In the following, we start from the selected  $bb\ell\ell$  events at SPS1a. The decay distribution is studied by generating events by using HERWIG[14], and simulate the events by using the ATLFAST detector simulator[15]. In order to minimize the combinatorial backgrounds we use the event pairings which satisfy the following conditions.

- Eq. (9) has solution for only one of the two possible lepton assignments.
- For the selected lepton assignment the resulting quartic equation in  $m_{\tilde{g}}^2$  has only two solutions, and the difference of the gluino masses for the two solutions is more than 100 GeV. The smaller gluino mass solution is chosen.

Note the selections are rather phenomenological and they may introduce some bias to the reconstructed sparticle masses.

The  $m_{\tilde{g}}$  distributions for the OSSF×OSSF events pairs are shown in the histograms on the upper line of Fig. 1. We find the obtained peak positions are consistent with the input masses in this

study. A significant SUSY background, also shown in Fig. 1 is still present in the sample. This background can be estimated from the data themselves by using the  $bb\ell\ell$  events with an opposite sign opposite flavor (OSOF) lepton pair (i.e.  $\ell\ell = e^{\pm}\mu^{\mp}$ ).

The histogram shows a peak corresponding to the input value for the gluino mass even before the background subtraction. The green and blue histograms show the estimated background distributions. The distributions after the background subtraction are shown in the histogram on the lower line of Fig. 1. The peak position and its error obtained by a Gaussian fit to the distribution are and it is  $591.9\pm0.7$  GeV at SPS1a. One can also look into the distribution of  $m_{\tilde{g}}-m_{\tilde{b}}$  and estimating the value of this observable by performing a Gaussian fit on the observed peak and the peak position is 98.9 GeV, while the input is 103.3 GeV.

The error of the peak position is O(1) GeV, but this is not the error of the gluino mass, because each event can be used many times for the mass calculation. To estimate the error, we generate many signal events at SPS1a(tan  $\beta = 10$ ) and study the deviation of the peak positions of the sub-samples. The gluino mass error for  $\int dt \mathcal{L} = 300 \text{fb}^{-1}$  is  $\Delta m_{\tilde{q}} \sim 2 \text{ GeV}$  at SPS1a.

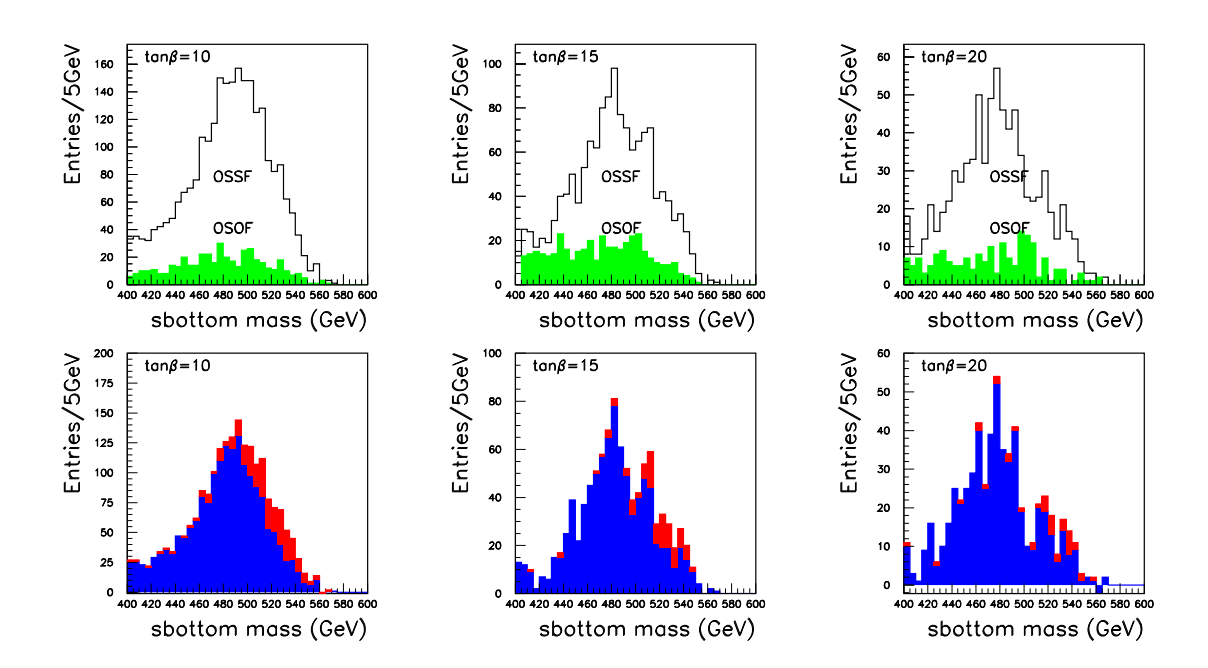


Figure 2: The  $m_{\tilde{b}}$  distributions for  $\tan\beta=10$  (left), 15 (center) and 20 (right) with a fixed gluino mass ( $m_{\tilde{g}}=595$  GeV). The open and green histograms in the top figures show the distributions of OSSF and OSOF lepton events, respectively. The mass distributions after background subtraction are shown in the bottom figures, where the contribution of the  $\tilde{b}_2$  events are shown by the red regions.

Once the gluino mass is fixed by the analysis shown above, Eq. (9) can be solved for each event for two solutions for the sbottom mass, giving as input the central measured value for the gluino mass. In Fig. 2, we plot the distribution of the smaller sbottom mass solution  $m_{\tilde{b}}(\min)$  for both OSSF (signal) and OSOF (background) lepton pair events (top histograms) for SPS1a and two other model points which has same MSUGRA parameters but  $\tan \beta = 15$  and 20. The relevant sparticles masses are listed in Table . The  $m_{\tilde{b}_1}$  changes sensitively with  $\tan \beta$  due to the increased left right mixing. We show in the bottom line the mass distributions after the background subtraction. The peak positions are evaluated by a Gaussian fit, and listed in Table 3. Note that the total number of the signal  $\tilde{b}_1$  event is smaller by factor of 4 for  $\tan \beta = 20$  compared with  $\tan \beta = 10$ . This is because the decay  $\tilde{\chi}_2^0 \to \tau \tilde{\tau}$  dominates as  $\tan \beta$  increases. Thanks to the peak structure of the distribution, the mass peak is still seen very clearly. The  $m_{\tilde{b}}(\min)$  peak and  $m_{\tilde{b}}(\text{input})$  are in good agreement, and it is not so for the larger solution  $m_{\tilde{b}}(\text{max})$ .

The peak positions of the distribution of the events originated from  $\tilde{b}_2$  decay are also consistent with  $\tilde{b}_2$  masses. The existence of  $\tilde{b}_2$  can be established only after understanding b jet smearing and  $\tilde{b}_1$  distribution correctly.

	$\tan \beta = 10$	$\tan \beta = 15$	$\tan \beta = 20$
$m_{\tilde{b}}(\text{true})$		485.3	478.8
$m_{\tilde{b}}(\min)$	$492.1 \pm 1.2$	$487.7 \pm 2.2$	$474.3 \pm 2.4$
$m_{\tilde{b}}(\max)$	$504.5 \pm 1.0$	$502.9 \pm 1.7$	$495.1 \pm 2.4$

Table 3: Fit results of the sbottom mass in GeV with a fixed gluino mass ( $m_{\tilde{q}} = 595 \text{ GeV}$ ).

## 2.4. Likelihood analysis

Because Eq. (9) have multiple solutions for a fixed gluino mass, we encountered the problem to select the one of the multiple solution artificially in the previous subsection. To avoid bias to the analysis, we introduce a "likelihood analysis" in this subsection.

From Eq. (9), each event is represented as a curve in the  $(m_{\tilde{g}}, m_{\tilde{b}})$  plane. The coefficients of the curve are a function of the four momenta of the detected partons. The partons are measured as jets in the detector, which smears the parton according to a smearing function. From the measured quadratic form for an event we can build a confidence belt in the  $(m_{\tilde{g}}, m_{\tilde{b}})$  plane[16,13]. In order to build the "probability distribution function", the crucial ingredient is the distribution of the measured b-jet momenta as a function of the b-parton momenta. We define an approximate probability density function according to the formula:

$$\mathcal{L}(m_{\tilde{g}}, m_{\tilde{b}}) = \int dp_1' \int dp_2' \epsilon(p_1 : p_1') \epsilon(p_2 : p_2') \delta(f(m_{\tilde{g}}, m_{\tilde{b}}, p_1', p_2'))$$
(10)

where  $\epsilon(p:p')$  is the probability to measure a momentum p' for a b jet, given a b-parton with momentum p.

In Eq. (10) we did not include the possibility of lepton momentum mis-measurement, which has an almost negligible effect. We also assume that the jet direction is not modified by the measurement and we use for  $\epsilon(p:p')$  a gaussian distribution, with a width  $\sigma$  corresponding to the parameterized jet smearing used in the fast simulation program. The approximate function takes however into account the dominant part of the jet smearing and can be used to demonstrate the method.

We now show numerically calculated  $\log \mathcal{L}$  in the  $(m_{\tilde{g}} - m_{\tilde{b}}, m_{\tilde{g}})$  plane for a few events where the  $bb\ell\ell$  events originates from the cascade decay of Eq. (7) at SPS1a. We calculate  $\mathcal{L}$  using the following procedure. For each event in our sample, characterized by a  $(p_1, p_2)$  pair of measured momenta for the b-jets, we generate Monte Carlo events of two b jets with momentum  $(p'_1, p'_2)$ , where  $p'_1$  and  $p'_2$  are randomly generated according to the function  $\epsilon(p_1 : p'_1) \times \epsilon(p_2 : p'_2)$ . The histgrams of the number of curves which satisfy Eq. (9) that go through 1 GeV×1 GeV grid in the  $(m_{\tilde{g}}, m_{\tilde{b}})$  plan, normalized by dividing the total generated event n corresponds to  $\mathcal{L}(m_{\tilde{g}}, m_{\tilde{b}})$ . In Fig. 3, we plot

$$\Delta \log \mathcal{L} = \log(\mathcal{L}(m_{\tilde{g}}, m_{\tilde{g}} + \Delta m_{\tilde{g}}, m_{\tilde{b}}, m_{\tilde{b}} + \Delta m_{\tilde{b}}) + c) - \log(\mathcal{L}(\min)), \tag{11}$$

where c = 0.001 is a constant cutoff factor, which is needed as for each event we generate only a finite number of Monte Carlo experiments, and therefore some bins can have

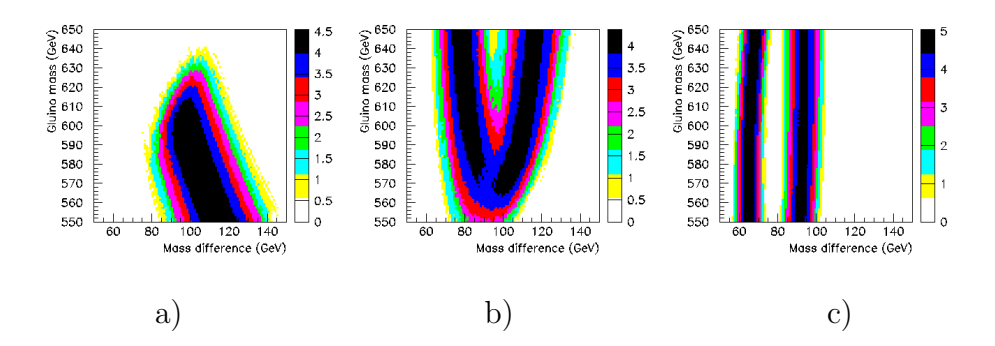


Figure 3: Likelihood distributions in the  $(m_{\tilde{g}} - m_{\tilde{b}}, m_{\tilde{g}})$  for selected events.

zero hits. The shape of the probability density distribution is different event by event, as it depends on the event kinematics. The size of the allowed band is also different, which means that some events will have more weight in the determination of the mass parameters.

By combining the probabilities for different events, a region of maximum probability in the  $(m_{\tilde{g}}, m_{\tilde{b}})$  is found, where the curves of maximum probability for all events approximately cross. Namely, we can build the combined likelihood for all the events defined as:

$$\log \mathcal{L}_{\text{comb}}(m_{\tilde{g}}, m_{\tilde{g}} + \Delta m_{\tilde{g}}, m_{\tilde{b}}, m_{\tilde{b}} + \Delta m_{\tilde{b}}) = \sum_{\text{events}} \log (\mathcal{L}(m_{\tilde{g}}, m_{\tilde{g}} + \Delta m_{\tilde{g}}, m_{\tilde{b}}, m_{\tilde{b}} + \Delta m_{\tilde{b}}) + c).$$
(12)

To study the likelihood distribution of gluino and sbottom mass, we actually shows the distribution of subtracted likelihood

$$\log \mathcal{L}_{\text{sub}} \equiv \log \mathcal{L}_{\text{OSSF}} - \log \mathcal{L}_{\text{OSOF}} \equiv \sum_{\text{OSSF}} \log \mathcal{L} - \sum_{\text{OSOF}} \log \mathcal{L}.$$
 (13)

This is not the correct definition of the likelihood function, but in the limit of infinite statistics,  $\log \mathcal{L}_{\text{sub}}$  is independent from the contribution of accidental lepton pairs. For the correct treatment, see [13].

We plot the contours of the function  $\log \mathcal{L}_{\text{sub}}$  in Fig. 4, where plots (a) and (b) [(c) and (d)] are for  $\tan \beta = 10$  [ $\tan \beta = 20$ ]. The distributions (a) and (c) are produced accepting all the events which pass the selections, whereas distributions (b) and (d) are produced using an event sample where the events including a  $\tilde{b}_2$  decay have been rejected.

In Fig. 4 (a) and (c), the position of the peak for  $m_{\tilde{g}} - m_{\tilde{b}}$  is roughly consistent with the input value. Unlike the gluino and sbottom mass fits in the previous section, we obtain the correct peak position without the need of artificially choosing among multiple solutions. The likelihood distribution can be used to determine the  $\tilde{g}$  and  $\tilde{b}$ . We restrict the likelihood distribution for 591 GeV  $< m_{\tilde{g}} < 599$  GeV (within 4 GeV from the input gluino mass). We then fit the distribution around the peak assuming gaussian distribution, The likelihood distribution peaks at the gluino and sbottom mass difference as 99.5 GeV for  $\tan \beta = 10$ , 104.2 GeV for  $\tan \beta = 15$ , and 113.9 GeV for  $\tan \beta = 20$ , where the input

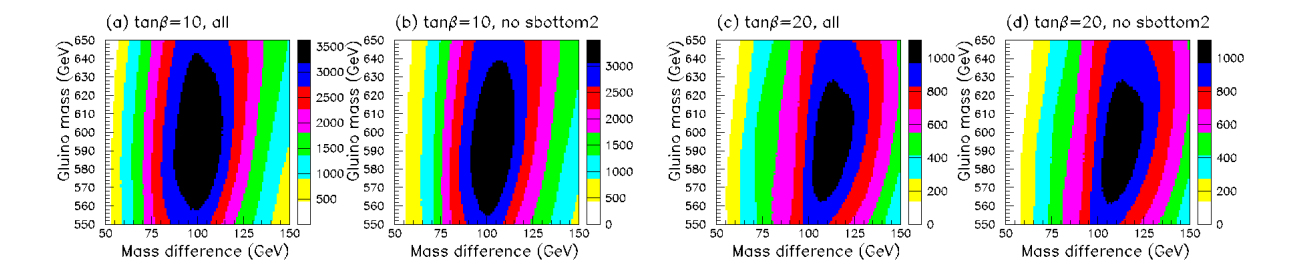


Figure 4: Contours of the likelihood function  $\log \mathcal{L}_{\text{sub}}$  in the  $(m_{\tilde{g}} - m_{\tilde{b}}, m_{\tilde{g}})$  plane: (a) for (c)  $\tan \beta = 10$  and (b) and (d) for  $\tan \beta = 20$ , respectively. The contours (b) and (d) are made without  $\tilde{b}_2$  contributions.

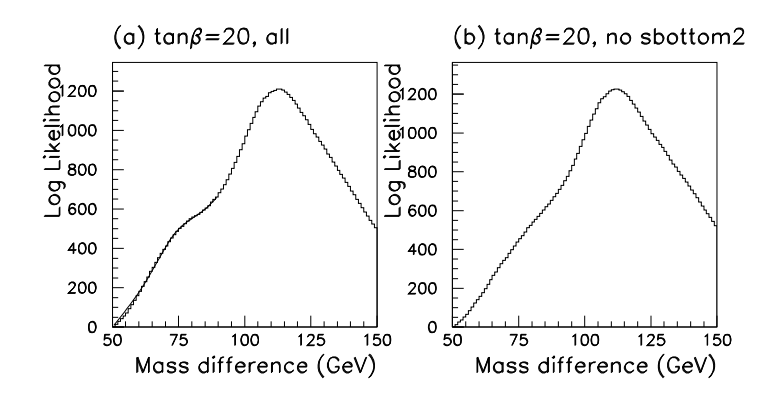


Figure 5: The likelihood as a function of  $m_{\tilde{g}} - m_{\tilde{b}}$  for  $\tan \beta = 20$ : (a) for all events and (b) without  $\tilde{b}_2$  events.

value is 103.3 GeV, 109.9 GeV and 116.5 GeV, respectively. The fitted values display shift of about 4 GeV from the true value. We ascribe this effect to our simplified modeling of the jet smearing in building the likelihood function, which should disappear once the detector response is properly taken into account in the unfolding procedure.

In Fig. 5(a), we show the distribution of  $\log \mathcal{L}_{\text{sub}}$  as a function of  $m_{\tilde{g}} - m_{\tilde{b}}$  at  $\tan \beta = 20$ , restricting the gluino mass in the region 591 GeV  $< m_{\tilde{g}} <$ 599 GeV again. On the left of the peak corresponding to the  $\tilde{b}_1$  mass, we see a small bump in the distribution. This bump is not observed in the mass distribution made without  $\tilde{b}_2$  contribution (Fig. 5(b)). In order to claim the presence of a second component in the distribution on the data, the ability of correctly reproducing the likelihood distribution for  $\tilde{b}_1$  events would be needed. It is also difficult to extract a statistical significance for the  $\tilde{b}_2$  shoulder as our definition of the likelihood function is approximate one.

## 2.5. More challenges

In the previous subsection, we have discussed the MSSM parameter determination at SPS1a. For this point, the mass spectrums would be obtained quite accurately by looking into the decay cascades involving leptons. The SUSY scale is relatively light  $m_{\tilde{q}} \sim m_{\tilde{q}} \sim 600$  GeV, when production cross section is as large as 50 pb. One can even

determine the edges of the  $\tilde{\chi}_4^0$  decays. If the squark and gluino mass scale is around 1 TeV, the production cross section is only around 3 pb, and statistical errors would be increased accordingly.

The sensitivity to the masses would be further reduced when  $m_{\tilde{q}} > m_{\tilde{g}}$ . For this case squarks decay dominantly into gluino, and the gluino decay is 3 body. Then it is hard to identify the jets from squark and gluino decays. This is typically the case for the model points in the "Focus point region" in the supergravity model.

The mass resolution also may be worse when  $\tan\beta$  is large in MSUGRA, because the branching ratios of the  $\tilde{\chi}^0_2$  into  $\mu$  or e are reduced significantly as  $Br(\tilde{\chi}^0_2 \to \tilde{\tau}\tau)$  dominates. The decay into  $\tau$  may also be studied, but a  $\tau$  jet resolution is significantly worse compared to that of a lepton, and the background are much higher due to fake  $\tau$ 's from QCD jets. The case where  $\tilde{\tau}$  and  $\tilde{\chi}^0_1$  are degenerated in mass is favored in MSUGRA model with the dark matter constraint, because the coannihilation of  $\tilde{\tau}$  and  $\tilde{\chi}^0_1$  reduces the thermal relic density in the Universe to the acceptable level. In that case, one of the  $\tau$  lepton from  $\tilde{\chi}^0_2$  decays may be too soft to be detected at the LHC.

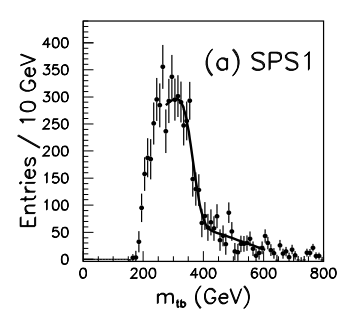
It is therefore important to establish analysis which does not relay on the leptons in the event cascades. For this purpose we discussed the reconstruction of the tb final state where top decays hadronically [17]. The dominant decay of gluinos for these points are  $\tilde{g} \to (\tilde{t}, \tilde{b}) \to tb\tilde{\chi}_i^{\pm}$ . The top quarks in the SUSY events may be reconstructed by looking for the bjj where  $m_{jj} \sim m_W$  and  $m_{bjj} \sim m_t$ . There are many accidental background which satisfy this conditions, because the number of jets  $n_{\text{jets}}$  in the SUSY events are typically 8 to 10. Such backgrounds can be subtructed by using the side band events where  $m_{ij} < m_W - 15$  GeV and  $m_{ij} > m_W + 15$  GeV. The reconstructed top quarks are then used to study the  $m_{tb}$  distributions. In Fig. 6, we show the  $m_{tb}$  distribution after the background subtruction for SPS1a and SPS2, where SPS2 corresponds to the focus point where  $m_{\tilde{q}} \sim 800$  GeV and  $m_{\tilde{q}_L} \sim 1.5$  TeV. For SPS1a,  $\tilde{g} \to \tilde{t}t$  and bb is open, and distribution shows sharp edge consistent to those calculated from the input masses. The endpoint is measured within an error  $\Delta m_{tb} \sim 4$  GeV, and the distribution maybe used to study the t nature. For the case of SPS2, the decay chain is not open, but gluino still dominantly decay into third generation particles because stop and sbottom masses are significantly lighter than that of the first and second generation squarks. The distribution does not show the edge structure because the gluino decay is three body. The  $m_{tb}$  endpoint is consistent to the mass difference  $m_{\tilde{g}} - m_{\tilde{\chi}_1^+} \sim 560 \text{ GeV}$  and  $m_{\tilde{g}} - m_{\tilde{\chi}_2^+} \sim 480 \text{ GeV}$ .

#### 3. Supersymmetric Relations

In MSSM, all dimensionless couplings involving supersymmetric particles are described by either SM Yukawa or gauge couplings. Not only the size of the couplings, but the chiral structure of the couplings are restricted by the supersymmetry. The fermionsfermion-gaugino coupling is restricted to preseve the chirality of (s)fermion, therefore for example,

$$\mathcal{L} = \frac{g}{\sqrt{2}} \left[ \overline{\tilde{W}} l_L \tilde{l}_L^* + \tan \theta_W \overline{\tilde{B}} l_L \tilde{l}_L^* - 2 \tan \theta_W \overline{\tilde{B}} f_R \tilde{f}_R^* + h.c. \right], \tag{14}$$

for the lepton-slepton-gaugino interaction, while the chirality must be flipped for the



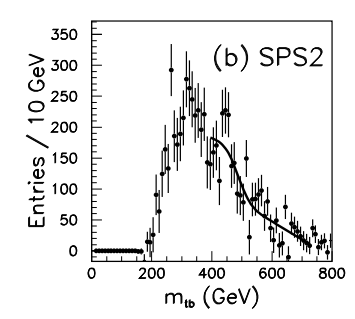


Figure 6: The  $m_{tb}$  distribution at SPS1a and SPS2. The formar is dominated by the two body cascade decay  $\tilde{g} \to t\tilde{t}, b\tilde{b} \to tb\tilde{\chi}_1^+$  and the latter is dominated by the three body decay  $\tilde{g} \to tb\tilde{\chi}_i^+$ .

Higgsino interactions. Proving the couplings and their chiral structures is important steps to check if the discovered new particles are indeed superpartners of the SM particles or not.

For some cases one can check the chiral structure of the interaction by looking into the decay distributions. We first note that the SUSY particles are naturally polarized in many SUSY process. For example, in the cascade decay

$$\tilde{q}_L \to \tilde{\chi}_2^0 q_L \to \tilde{l}_R l_R q \to l l q \tilde{\chi}_1^0,$$
 (15)

the  $\tilde{\chi}_2^0$  is polarized as right-handed (opposite to  $q_L$ ), because the Yukawa coupling of squark-quark-ino flip the chirality. The polarized  $\tilde{\chi}_2^0$  further decay into either leptons-antislepton, or antilepton-slepton. The two decay branching ratios are same because  $\tilde{\chi}_2^0$  is a Majorana particles. For the decay  $\tilde{\chi}_2^0 \to \tilde{l}_R l^+$  through Yukawa type interaction, antilepton likely to go in the same direction to  $\tilde{\chi}_2^0$  (namely opposite to the jets in the squark rest flame), while the lepton goes in the same direction to the jet for the  $\tilde{\chi}_2^0 \to \tilde{l}_R^* l^-$  decay.

The difference of the angular distribution appears as the charge asymmetry in the m(jl) distribution[18], because the m(jl) is proportional to  $1 - \cos \theta$ , where  $\theta$  is the angle between the jets and the lepton in the  $\tilde{\chi}_2^0$  rest flame. The  $m(jl^+)$  is peaked sharply at the endpoint of m(jl) distribution, while the  $m(jl^-)$  distribution is suppressed at the endpoint. Finally a (anti)lepton is emitted from a (anti)slepton, but this time the lepton angle distribution is spherical in the  $\tilde{l}$  rest flame.

The charge asymmetry is exactly opposite for  $\tilde{q}_L^*$  decays. However, at pp colliders, the number of produced squark is much larger than that of anti-squark, and the  $\tilde{\chi}_2^0$  produced from  $\tilde{q}_L$  decay dominates total  $\tilde{\chi}_2^0$  productions. The charge asymmetry in m(jl) distribution in the jll sample therefore remains. From the distribution, one can conclude that the decay products  $\tilde{\chi}_2^0$  is a fermionic particle, and the interaction is chiral[19,20].

The detectability of the charge asymmetry can be studied by generating events by using HERWIG[14], and simulate the events by using the ATLFAST detector simulator[15]. Here we show two representative case at the points SPS1a and SPS3 in Fig. 7, where the decay  $\tilde{\chi}_2^0 \to l\tilde{l}_R$  dominates at SPS1a and  $l\tilde{l}_L$  dominates at SPS3 respectively. The distributions shows opposite asymmetry near the endpoints the m(jl) distributions for

the decay  $\tilde{q} \to q\tilde{\chi}_2^0 \to ql\tilde{l}$  (298 GeV at SPS1a and 200 GeV at SPS3 respectively). This is because the chirality of the  $\tilde{\chi}_2^0$ -l- $\tilde{l}$  coupling is exactly opposite for the two points[20].

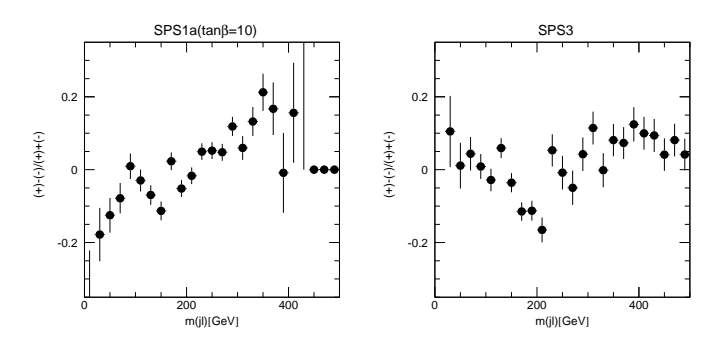


Figure 7: The reconstructed asymmetry  $[N_{\text{sig}}(jl^+) - N_{\text{sig}}(jl^-)]/[N_{\text{sig}}(jl^+) + N_{\text{sig}}(jl^-)].$ 

The cascade decay may also be sensitive to the  $\tilde{l}_L$  and  $\tilde{l}_R$  mixing[20]. Due to the F term contribution of slepton mass matrix,  $m_{LR}^2 \sim m_f \mu \tan \beta$ , the lighter slepton mass eigenstates  $\tilde{l}_1$  is mixture of  $\tilde{l}_L$  and  $\tilde{l}_R$  where the mixing angle is defined as  $\tilde{l}_1 = \tilde{l}_L \cos \theta_l + \tilde{l}_R \sin \theta_l$ . The left and right hand coupling of the  $\tilde{\chi}_2^0$  to the lighter mass eigenstate  $l_1$  is expressed as

$$\mathcal{L} = -\frac{g_2}{\sqrt{2}} \tilde{\chi}_2^0 (C_L P_L l + C_R P_R l) \tilde{l}_1^*, 
C_L \equiv -\cos \theta_l (N_{\tilde{W}2}^* + N_{\tilde{B}2}^* \tan \theta_W), 
C_R \equiv 2 \tan \theta_W \sin \theta_l N_{\tilde{B}2},$$
(16)

when  $\tilde{\chi}_2^0$  is gaugino like.

When  $\tilde{\chi}_2^0 \sim \tilde{W}$ ,  $\tilde{\chi}_1^0 \sim \tilde{B}$ , and  $\tilde{l}_1 \sim \tilde{l}_R$ ,  $C_L$  is suppressed by small mixing angle proportional to  $m_f \mu \tan \beta$ , while  $C_R$  is suppressed by the small bino component of the wino like  $\tilde{\chi}_2^0$ . The non-universality appears as the sign of the non-zero F term mixing of  $\tilde{\mu}$  and visible in the wide parameter region.

While the mixing angle of  $\tilde{\mu}$  is only around 1% for the Snowmass point SPS1a, the difference of the decay branching ratio  $Br(\tilde{\chi}_2^0 \to \tilde{\mu}\mu)/Br(\tilde{\chi}_2^0 \to \tilde{e}\mu)$  from 1 is as large as 4%. Although the statistics reduces as  $\tan\beta$  increases, statistical significance of the signal defined as

$$S = \left(\frac{Br(\mu)}{Br(e)} - 1\right) \left(\frac{\Delta N(\text{sig})}{N(\text{sig})}\right)^{-1}$$

where  $\Delta N(\text{sig}) = \sqrt{N_{\text{OS}}}$ , and  $N_{\text{OS}}$  is the number of the total odd sign two lepton events. We found that S increase from 5.4 at SPS1a to 8.5 for a modified point with  $\tan \beta = 20$  (see Table 4).

### 4. Discussion

In this talk, we discussed SUSY studies at the LHC. In early '90, the LHC was considered merely as a discovery machine, due to the challenging experimental environment.

point	$Br(\tilde{\chi}_2^0 \to e\tilde{e})$	$N_{\rm sig}(e \text{ and } \mu)$	$N_{\mathrm{OS}}$	$\left(\frac{Br(\mu)}{Br(e)}-1\right)$	S
$\tan \beta = 10$	6.3%	$1.39 \times 10^{4}$	$2.68 \times 10^4$	4%	5.4
$\tan \beta = 20$	1.2%	$0.28 \times 10^4$	$1.02 \times 10^4$	17%	8.5

Table 4: The  $Br(\tilde{\chi}_2^0 \to e\tilde{e})$  and accepted number of events for SPS1a  $\tan \beta = 10, 20$ .  $N_{\rm sig}$  is the number of  $l^+l^-$  events after  $e^{\pm}\mu^{\mp}$  subtraction, while  $N_{\rm OS}$  is the number of the total odd sign two lepton events. The expected deviation of  $Br(\tilde{\chi}_2^0 \to \tilde{\mu}\mu)$  from that for  $\tilde{e}e$  is compared with the statistical error of the number of the  $e^+e^-$  events for  $\int dt \mathcal{L} = 300 \text{ fb}^{-1}$ .

However, it was recognized that the parameters of the MSSM can be determined at the LHC. Since then, many techniques have been developed to extract the mass and coupling information.

When the gravitino is the LSP and the NLSP is long lived, the LHC works as the machine for precision studies. This is because SUSY events contains many leptons and photons whose momentum can be easily combined to solve sparticle masses. For the case of the charged NLSP, the semi-stable charged particles would be observed as a highly ionizing charged tracks which goes through the detector. The decay position and decay time of the NLSP can be measured at the LHC, and the gravitino interaction to the matter may be explored. The cosmology related to the gravitino LSP and the collider phenomenology have received lots of attentions.

When the LSP is the lightest neutralino, the sparticle mass determination using the endpoint analysis is known to be very powerful. For the most favorable case, one can determine the LSP mass within 5% and squark and gluino masses within 2%. We have also introduced the mass relation method developed very recently in this talk. By using this method, one can reconstruct sparticle masses as peaks in the distributions calculated from the events using the exact formula to solve decay kinematics. The mass relation method may be useful even if the event statistics is small.

Finally we discussed the study of the sparticle interaction at the LHC. The chiral structure of the sparticle couplings may be studied through the charge asymmetry of the selected m(jl) distributions, where the jet and the lepton come from the cascade decay  $\tilde{q}_L \to \tilde{\chi}_2^0 q \to \tilde{l} l q$ .

To complete the task to explore all masses and couplings of SUSY particles is probably impossible by the LHC alone. However even after the ILC is started, the measurements at the LHC are useful to understand supersymmetry in nature. There are many on-going studies, and we still need more ideas and thoughts so that we do not miss any new physics signatures at the LHC.

## 5. References

- [1] ATLAS Collaboration, ATLAS detector and physics performance Technical Design Report, CERN/LHCC 99-14/15 (1999).
- [2] G. F. Giudice and R. Rattazzi, Phys. Rept. **322**, 419 (1999) [arXiv:hep-ph/9801271].

- [3] I. Hinchliffe and F. E. Paige, Phys. Rev. D **60**, 095002 (1999) [arXiv:hep-ph/9812233].
- [4] J. Feng, talk in this conference.
- [5] K. Hamaguchi, talk in this conference.
- [6] K. Hamaguchi, Y. Kuno, T. Nakaya and M. M. Nojiri, arXiv:hep-ph/0409248.
- [7] J. L. Feng and B. T. Smith, arXiv:hep-ph/0409278.
- [8] K. Kawagoe, T. Kobayashi, M. M. Nojiri and A. Ochi, Phys. Rev. D 69, 035003 (2004) [arXiv:hep-ph/0309031].
- [9] B. C. Allanach et al., in Proc. of the APS/DPF/DPB Summer Study on the Future of Particle Physics (Snowmass 2001) ed. N. Graf, Eur. Phys. J. C 25 (2002) 113
   [eConf C010630 (2001) P125] [arXiv:hep-ph/0202233].
- [10] B.K. Gjelsten, E. Lytken, D.J. Miller, P. Osland, and G. Polesello, ATLAS internal note ATL-PHYS-2004-007.
- [11] K. Desch, J. Kalinowski, G. Moortgat-Pick, M. M. Nojiri and G. Polesello, JHEP **0402**, 035 (2004) [arXiv:hep-ph/0312069].
- [12] M. M. Nojiri, G. Polesello and D. R. Tovey, arXiv:hep-ph/0312317.
- [13] K. Kawagoe, M. M. Nojiri and G. Polesello, arXiv:hep-ph/0410160.
- [14] G. Corcella et al., JHEP **0101**, 010 (2001) [arXiv:hep-ph/0011363].
- [15] E. Richter-Was, D. Froidevaux, and L. Piggishly, ATLAS internal note ATL-PHYS-98-131.
- [16] C.G. Lester "Building on a Proposal for a New Reconstruction Technique for SUSY processes at the LHC." in B. C. Allanach *et al.* [Beyond the Standard Model Working Group Collaboration], "Les Houches 'Physics at TeV Colliders 2003' Beyond the Standard Model Working Group: Summary report," arXiv:hep-ph/0402295.
- [17] J. Hisano, K. Kawagoe and M. M. Nojiri, Phys. Rev. D **68**, 035007 (2003) [arXiv:hep-ph/0304214].
- [18] P. Richardson, JHEP **0111**, 029 (2001) [arXiv:hep-ph/0110108].
- [19] A. J. Barr, Phys. Lett. B **596**, 205 (2004) [arXiv:hep-ph/0405052].
- [20] T. Goto, K. Kawagoe and M. M. Nojiri, arXiv:hep-ph/0406317.